

# Heavy Flavor and Quarkonium Production in pQCD

R. Vogt

Lawrence Livermore National Laboratory, Livermore, CA, USA

Physics Department, University of California, Davis, CA, USA

# Open Heavy Flavors

# Calculating Heavy Flavors in Perturbative QCD

‘Hard’ processes have a large scale in the calculation that makes perturbative QCD applicable: high momentum transfer,  $\mu^2$ , high mass,  $m$ , high transverse momentum,  $p_T$ , since  $m \neq 0$ , heavy quark production is a ‘hard’ process

Asymptotic freedom assumed to calculate the interactions between two hadrons on the quark/gluon level but the confinement scale determines the probability of finding the interacting parton in the initial hadron

Factorization assumed between the perturbative hard part and the universal, non-perturbative parton distribution functions

Hadronic cross section in an  $AB$  collision where  $AB = pp, pA$  or nucleus-nucleus is

$$\sigma_{AB}(S, m^2) = \sum_{i,j=q,\bar{q},g} \int_{4m_Q^2/s}^1 \frac{d\tau}{\tau} \int dx_1 dx_2 \delta(x_1 x_2 - \tau) f_i^A(x_1, \mu_F^2) f_j^B(x_2, \mu_F^2) \widehat{\sigma}_{ij}(s, m^2, \mu_F^2, \mu_R^2)$$

$f_i^A$  are the nonperturbative parton distributions, determined from fits to data,  $x_1$  and  $x_2$  are the fractional momentum of hadrons  $A$  and  $B$  carried by partons  $i$  and  $j$ ,  $\tau = s/S$

$\widehat{\sigma}_{ij}(s, m^2, \mu_F^2, \mu_R^2)$  is hard partonic cross section calculable in QCD in powers of  $\alpha_s^{2+n}$ : leading order (LO),  $n = 0$ ; next-to-leading order (NLO),  $n = 1 \dots$

Results depend strongly on quark mass,  $m$ , factorization scale,  $\mu_F$ , in the parton densities and renormalization scale,  $\mu_R$ , in  $\alpha_s$

# Choosing Parameters

Two important parameters: the quark mass  $m$  and the scale  $\mu$  – at high energies, far from threshold, the low  $x$ , low  $\mu$  behavior of the parton densities determines the charm result, bottom less sensitive to parameter choice

The scale is usually chosen so that  $\mu_F = \mu_R$ , as in parton density fits, no strict reason for doing so for heavy flavors

Two ways to make predictions:

Fit to Data (RV, Hard Probes Collaboration): fix  $m$  and  $\mu \equiv \mu_F = \mu_R \geq m$  to data at lower energies and extrapolate to unknown regions – favors lower  $m$

Uncertainty Band (Cacciari, Nason and RV): band determined from mass range,  $1.3 < m < 1.7$  GeV (charm) and  $4.5 < m < 5$  GeV (bottom) with  $\mu_F = \mu_R = m$ , and range of scales relative to central mass value,  $m = 1.5$  GeV (charm) and 4.75 GeV (bottom):  $(\mu_F/m, \mu_R/m) = (1, 1), (2, 2), (0.5, 0.5), (0.5, 1), (1, 0.5), (1, 2), (2, 1)$  (Ratio is relative to  $m_T$  for distributions)

Need to be careful with  $\mu_F \leq m$  and the CTEQ6M parton densities since  $\mu_{\min} = 1.3$  GeV, gives big  $K$  factors for low scales – problem occurs at low  $p_T$

Densities like GRV98 have lower  $\mu_{\min}$  so low  $x$ , low  $\mu$  behavior less problematic

Value of two-loop  $\alpha_s$  is big for low scales, for  $m = 1.5$  GeV:

$\alpha_s(m/2 = 0.75 \text{ GeV}) = 0.648$ ,  $\alpha_s(m = 1.5 \text{ GeV}) = 0.348$  and  $\alpha_s(2m = 3 \text{ GeV}) = 0.246$

## FONLL Calculation (Cacciari and Nason)

Designed to cure large logs of  $p_T/m$  for  $p_T \gg m$  in fixed order calculation (FO) where mass is no longer only relevant scale

Includes resummed terms (RS) of order  $\alpha_s^2(\alpha_s \log(p_T/m))^k$  (leading log – LL) and  $\alpha_s^3(\alpha_s \log(p_T/m))^k$  (NLL) while subtracting off fixed order terms retaining only the logarithmic mass dependence (the “massless” limit of fixed order (FOM0)), both calculated in the same renormalization scheme

Scheme change needed in the FO calculation since it treats the heavy flavor as heavy while the RS approach includes the heavy flavor as an active light degree of freedom

Schematically:

$$\text{FONLL} = \text{FO} + (\text{RS} - \text{FOM0}) G(m, p_T)$$

$G(m, p_T)$  is arbitrary but  $G(m, p_T) \rightarrow 1$  as  $m/p_T \rightarrow 0$  up to terms suppressed by powers of  $m/p_T$

Total cross section similar to but slightly higher than NLO

Problems at high energies away from midrapidity due to small  $x$ , high  $z$  behavior of fragmentation functions in RS result, therefore we don't calculate results for  $|y| > 2$ , worse for LHC predictions

# Comparison of FONLL and NLO $p_T$ Distributions

FONLL result for bare charm is slightly higher over most of the  $p_T$  range – fixed order result gets higher at large  $p_T$  due to large  $\log(p_T/m)$  terms

New  $D^0$  fragmentation functions (dashed) harder than Peterson function (dot-dot-dot-dashed)

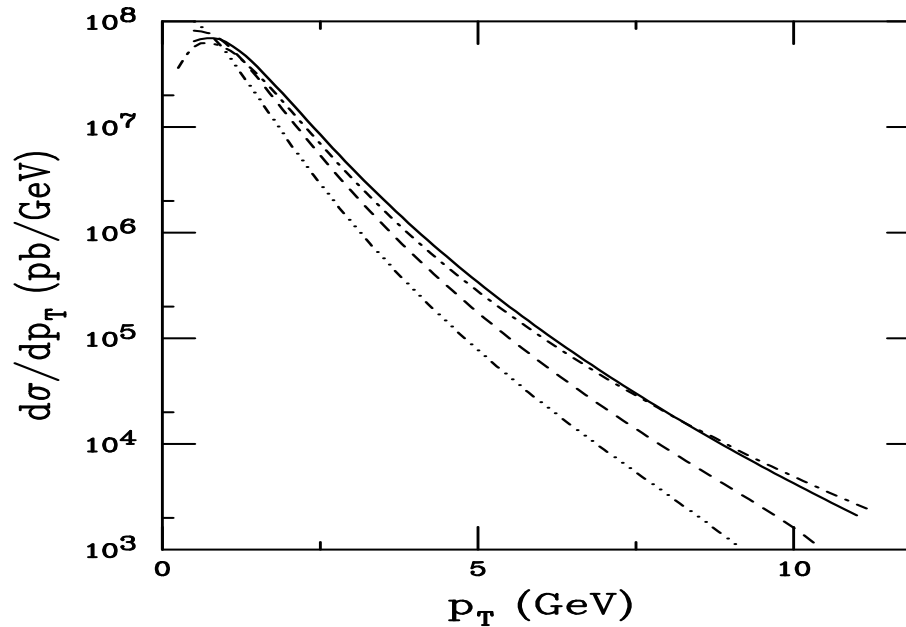


Figure 1: The  $p_T$  distributions calculated using FONLL are compared to NLO. The dot-dashed curve is the NLO charm quark  $p_T$  distribution. The solid, dashed and dot-dot-dot-dashed curves are FONLL results for the charm quark and  $D^0$  meson with the updated fragmentation function and the Peterson function, respectively. All the calculations are done with the CTEQ6M parton densities,  $m = 1.2$  GeV and  $\mu = 2m_T$  in the region  $|y| \leq 0.75$ .

# Uncertainty Bands for $p_T$ Distributions

Due to range of parameters chosen for uncertainty band, the maximum and minimum result as a function of  $p_T$  may not come from a single set of parameters

Thus the upper and lower curves in the band do not represent a single set of  $\mu_R$ ,  $\mu_F$  and  $m$  values but are the upper and lower limits of mass and scale uncertainties added in quadrature:

$$\frac{d\sigma_{\max}}{dp_T} = \frac{d\sigma_{\text{cent}}}{dp_T} + \sqrt{\left(\frac{d\sigma_{\mu,\max}}{dp_T} - \frac{d\sigma_{\text{cent}}}{dp_T}\right)^2 + \left(\frac{d\sigma_{m,\max}}{dp_T} - \frac{d\sigma_{\text{cent}}}{dp_T}\right)^2}$$

$$\frac{d\sigma_{\min}}{dp_T} = \frac{d\sigma_{\text{cent}}}{dp_T} - \sqrt{\left(\frac{d\sigma_{\mu,\min}}{dp_T} - \frac{d\sigma_{\text{cent}}}{dp_T}\right)^2 + \left(\frac{d\sigma_{m,\min}}{dp_T} - \frac{d\sigma_{\text{cent}}}{dp_T}\right)^2}$$

The central values are  $m = 1.5$  GeV (charm) and 4.75 GeV (bottom),  $\mu_F = \mu_R = m_T$

Previous (HPC) charm results with  $m = 1.2$  GeV,  $\mu_F = \mu_R = 2m_T$  fall within the uncertainty band

Bare heavy quark and heavy flavor meson  $p_T$  distributions shown for  $pp$  collisions at  $\sqrt{S} = 200$

# Components of Uncertainty Band at NLO

Curves with  $(\mu_F/m_T, \mu_R/m_T) = (1, 0.5)$  and  $(0.5, 0.5)$  define the maximum of the band with  $(0.5, 1)$  and  $(2, 2)$  form the minimum

Turnover of minimum at low  $p_T$  because  $\mu_F < \mu_{\min}$  of CTEQ6M

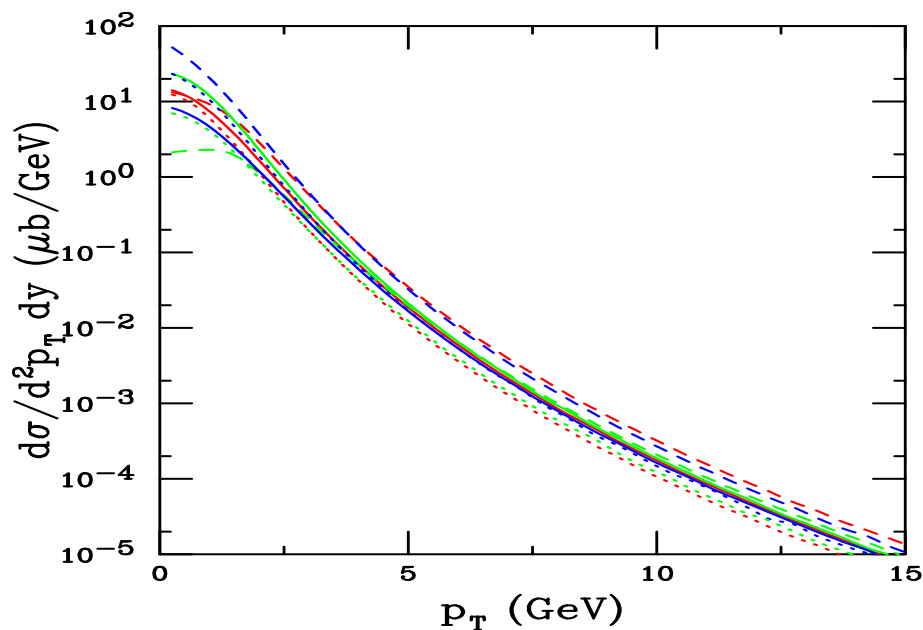


Figure 2: The charm quark  $p_T$  distributions calculated using CTEQ6M. The solid red curve is the central value  $(\mu_F/m_T, \mu_R/m_T) = (1, 1)$  with  $m = 1.5$  GeV. The green and blue solid curves are  $m = 1.3$  and  $1.7$  GeV with  $(1, 1)$  respectively. The red, blue and green dashed curves correspond to  $(0.5, 0.5)$ ,  $(1, 0.5)$  and  $(0.5, 1)$  respectively while the red, blue and green dotted curves are for  $(2, 2)$ ,  $(1, 2)$  and  $(2, 1)$  respectively, all for  $m = 1.5$  GeV.

# Uncertainty Bands for $c$ and $b$ at 200 GeV

Not possible to separate  $c$  and  $D$  bands for  $p_T < 10$  GeV – looks more like a delta function

Larger uncertainty bands for  $c$  and  $D$  than  $b$  and  $B$

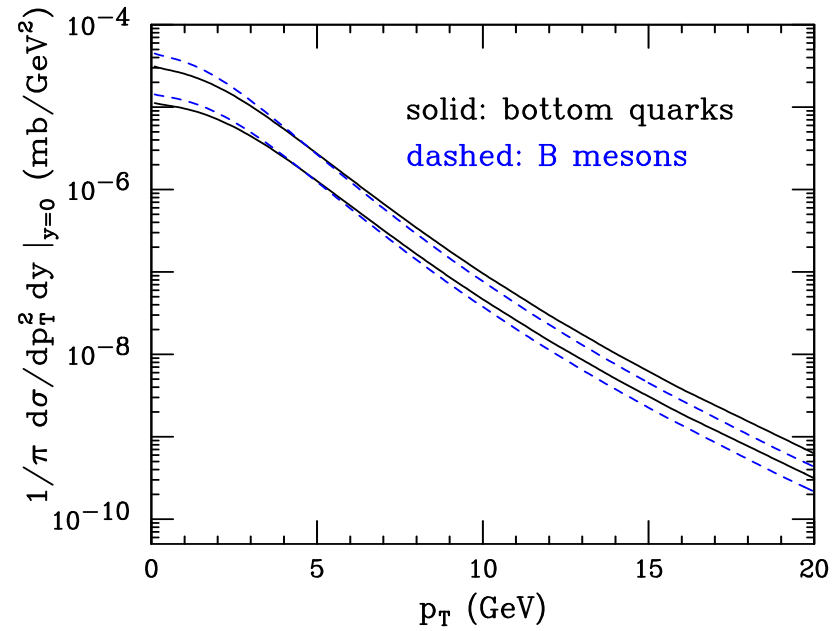
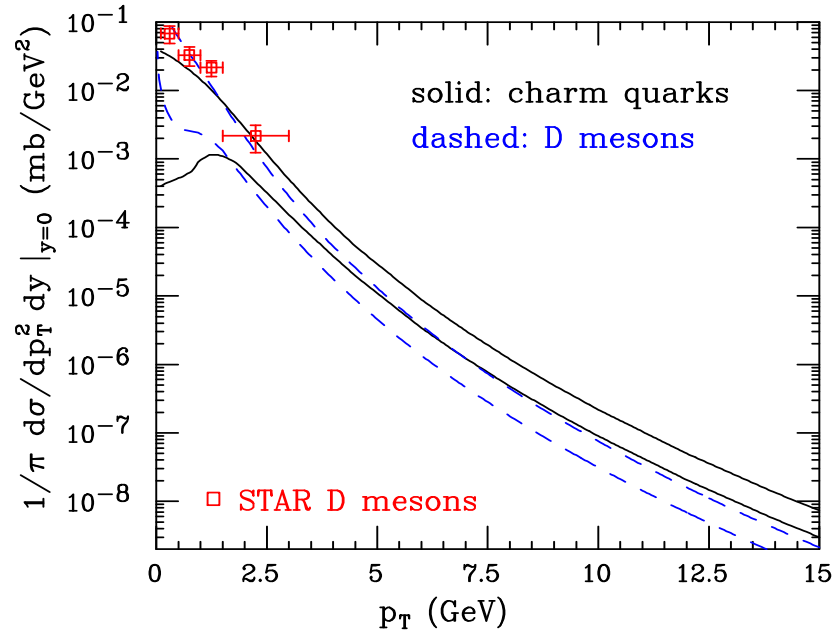


Figure 3: Left-hand side: The theoretical uncertainty bands for  $c$  quark and  $D$  meson  $p_T$  distributions in  $pp$  collisions at  $\sqrt{s} = 200$  GeV, using  $\text{BR}(c \rightarrow D) = 1$ . The final STAR d+Au data (scaled to  $pp$  using  $N_{\text{coll}} = 7.5$ ) are also shown. Right-hand side: The same for  $b$  quarks and  $B$  mesons.

# Obtaining the Electron Spectra From Heavy Flavor Decays

$D$  and  $B$  decays to leptons depends on measured decay spectra and branching ratios

$D \rightarrow e$  Use preliminary CLEO data on inclusive electrons from semi-leptonic  $D$  decays, assume it to be indentical for all charm hadrons

$B \rightarrow e$  Primary  $B$  decays to electrons measured by Babar and CLEO, fit data and assume fit to work for all bottom hadrons

$B \rightarrow D \rightarrow e$  Obtain electron spectrum from convolution of  $D \rightarrow e$  spectrum with parton model calculation of  $b \rightarrow c$  decay

Branching ratios are admixtures of charm and bottom hadrons

$$B(D \rightarrow e) = 10.3 \pm 1.2\%$$

$$B(B \rightarrow e) = 10.86 \pm 0.35\%$$

$$B(B \rightarrow D \rightarrow e) = 9.6 \pm 0.6\%$$

# Uncertainty Bands for Electrons from Heavy Flavor Decays at 200 GeV

Electrons from  $B$  decays begin to dominate at  $p_T \sim 5$  GeV

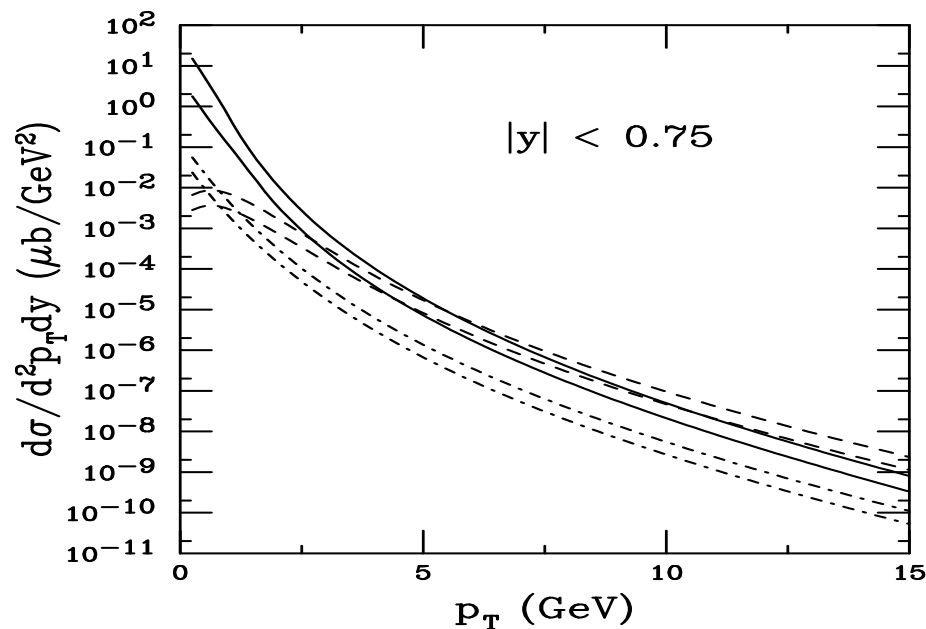


Figure 4: Left-hand side: The theoretical uncertainty bands for  $D \rightarrow e$  (solid),  $B \rightarrow e$  (dashed) and  $B \rightarrow D \rightarrow e$  (dot-dashed) as a function of  $p_T$  in  $\sqrt{s} = 200$  GeV  $pp$  collisions for  $|y| < 0.75$ . Right-hand side: The final electron uncertainty band in  $pp$  collisions is compared to the PHENIX and STAR (final and preliminary) data.

# Location of $b/c$ Crossover Sensitive to Details of Fragmentation Scheme, Scales, Quark Mass

The  $b \rightarrow e$  decays dominate already at lower  $p_T$  when standard Peterson function fragmentation ( $\epsilon_c = 0.06, \epsilon_b = 0.006$ ) is used since it hardens charm  $p_T$  spectra more than bottom

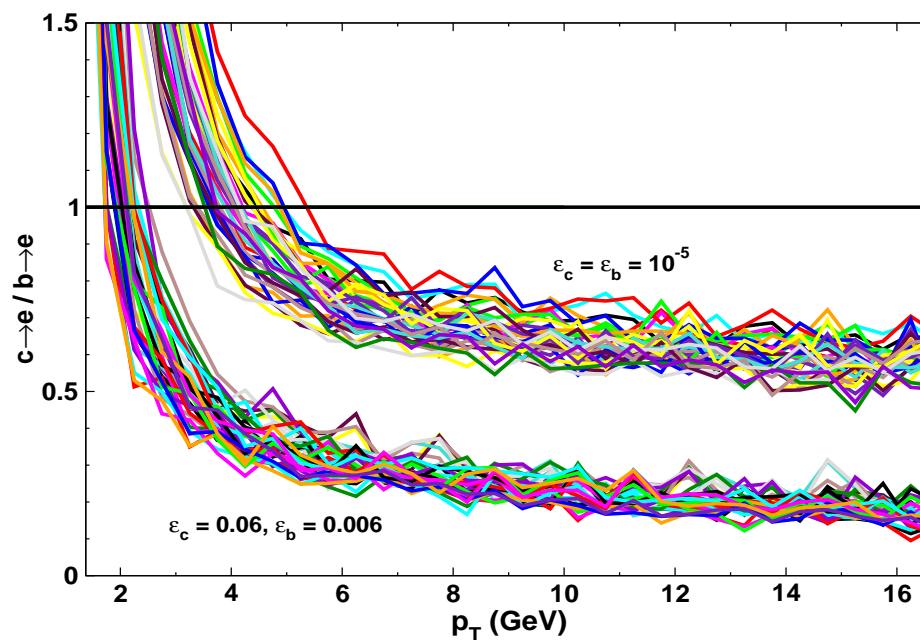


Figure 5: The ratio of charm to bottom decays to electrons obtained by varying the quark mass and scale factors. The effect of changing the Peterson function parameters from  $\epsilon_c = 0.06, \epsilon_b = 0.006$  (lower band) to  $\epsilon_c = \epsilon_b = 10^{-5}$  (upper band) is also illustrated. (From M. Djordjevic *et al.*)

# Comparison to Electron Data at 200 GeV

Includes PHENIX preliminary data from  $pp$  and STAR published and preliminary data

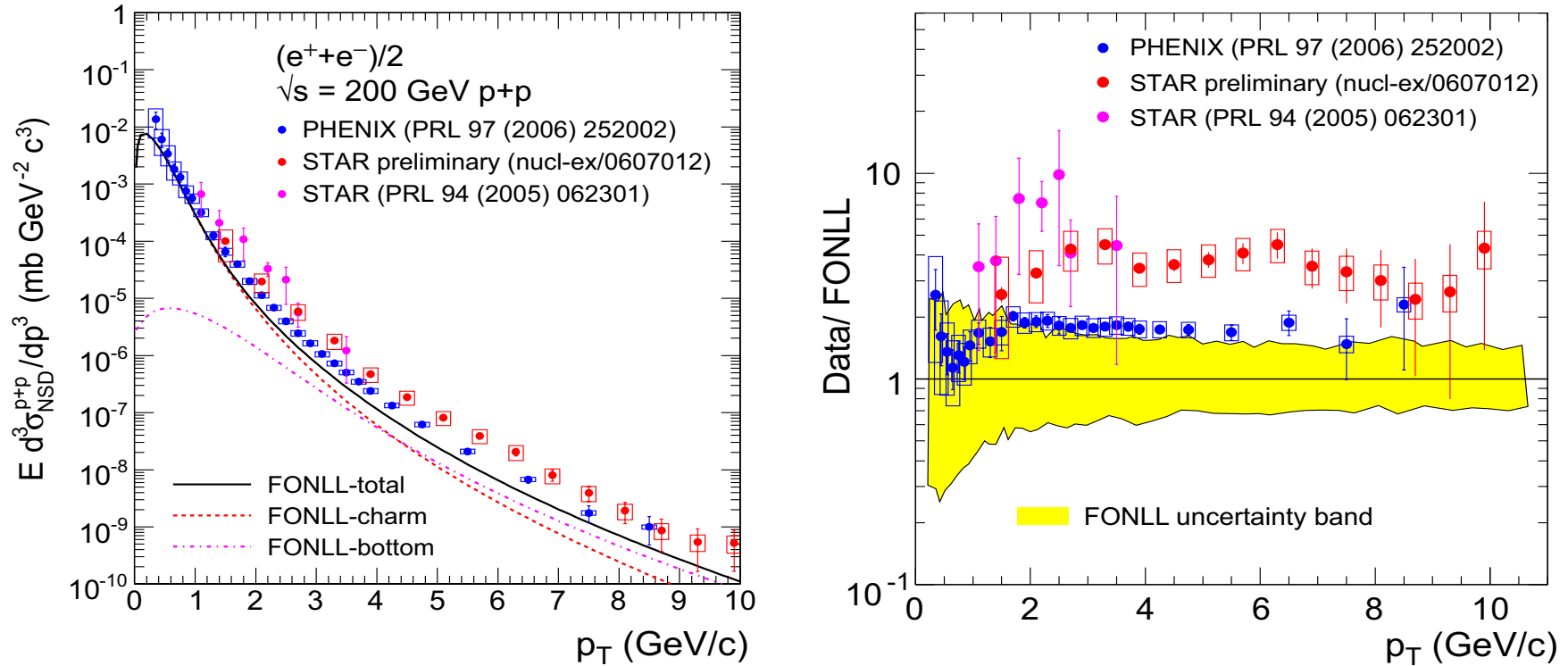


Figure 6: Left: Compilation of PHENIX and STAR measurements of the  $p_T$  dependence of the semileptonic decay open heavy flavor cross section from 200 GeV  $pp$  collisions, compared with FONLL calculations. Right: The ratio of the data to the FONLL calculation. The band depicts the theoretical uncertainty of the calculation.

## Open Heavy Flavor Summary

- The FONLL calculation of heavy quark production is used to better predict the  $p_T$  dependence at collider energy – cures large logs of  $p_T/m$
- Includes more modern fragmentation functions for  $D$  and  $B$  mesons – meson and quark distributions similar at higher  $p_T$  than previously obtained from older  $e^+e^-$  fits
- Contributions of  $D$  and  $B$  decays to leptons difficult to disentangle, requires reconstruction of hadronic decays to distinguish between them
- STAR and PHENIX measure same shape for single electron spectra, agrees with FONLL prediction, difference lies in normalization: the issue still needs to be resolved

# Quarkonium

# Production in Color Evaporation Model (CEM)

Gavai *et al.*, G. Schuler and R.V.

All quarkonium states are treated like  $Q\bar{Q}$  below  $H\bar{H}$  threshold

Distributions  $(x_F, p_T, \sqrt{s}, A)$  for all quarkonium family members identical — leads to constant ratios

At LO,  $gg \rightarrow Q\bar{Q}$  and  $q\bar{q} \rightarrow Q\bar{Q}$ ; NLO add  $gq \rightarrow Q\bar{Q}q$

$$\sigma_C^{\text{CEM}} = F_C \sum_{i,j} \int_{4m^2}^{4m_H^2} d\hat{s} \int dx_1 dx_2 f_{i/p}(x_1, \mu^2) f_{j/p}(x_2, \mu^2) \hat{\sigma}_{ij}(\hat{s}) \delta(\hat{s} - x_1 x_2 s)$$

$F_C$  fixed at NLO from total cross section data as a function of  $\sqrt{s}$ ,  $\sigma(x_F > 0)$  for inclusive  $J/\psi$  and  $B_{\mu\mu} d\sigma(\Upsilon + \Upsilon' + \Upsilon'')_{y=0}/dy$

Values of  $m$  and  $\mu$  (here  $\mu \propto \sqrt{(p_{TQ}^2 + p_{T\bar{Q}}^2)/2 + m_Q^2} = m_{TQ\bar{Q}} \equiv m_T$  in the exclusive  $Q\bar{Q}$  code) for several parton densities fixed from  $Q\bar{Q}$  production

We don't use NRQCD to study shadowing and absorption at LHC since total cross section matrix elements needed are fit to CTEQ3L (obsolete) parton densities – would need to refit matrix elements with more recent PDF set better behaved at low  $x$

# Production and Feed Down Fractions

Data and branching ratios can be used to separate out the  $F_C$ 's for each state in quarkonium family

Resonance	$\sigma_i^{\text{dir}}/\sigma_H$	$f_i$
$J/\psi$	<b>0.62</b>	<b>0.62</b>
$\psi'$	<b>0.14</b>	<b>0.08</b>
$\chi_{c1}$	<b>0.6</b>	<b>0.16</b>
$\chi_{c2}$	<b>0.99</b>	<b>0.14</b>
$\Upsilon$	<b>0.52</b>	<b>0.52</b>
$\Upsilon'$	<b>0.33</b>	<b>0.10</b>
$\Upsilon''$	<b>0.20</b>	<b>0.02</b>
$\chi_b(1P)$	<b>1.08</b>	<b>0.26</b>
$\chi_b(2P)$	<b>0.84</b>	<b>0.10</b>

Table 1: The ratios of the direct quarkonium production cross sections,  $\sigma_i^{\text{dir}}$ , to the inclusive  $J/\psi$  and  $\Upsilon$  cross sections, denoted  $\sigma_H$ , and the feed down contributions of all states to the  $J/\psi$  and  $\Upsilon$  cross sections,  $f_i$ .

# $J/\psi$ and $\Upsilon$ NLO CEM Cross Sections

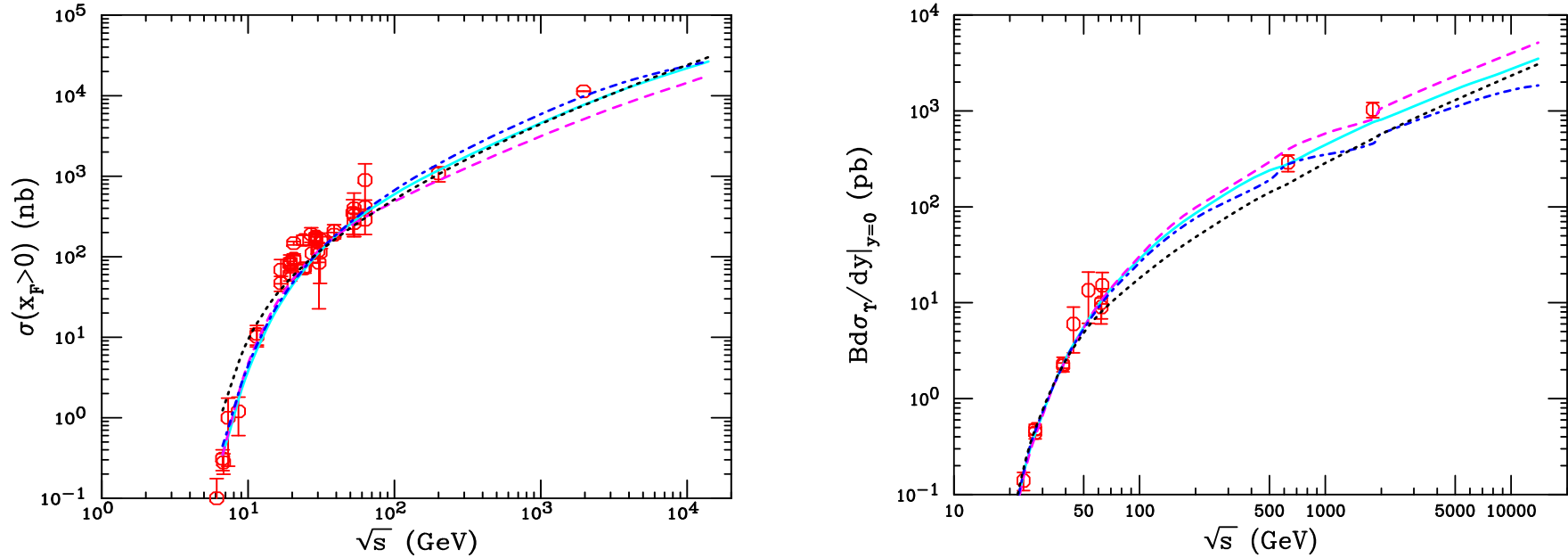


Figure 7: (Left) The NLO  $J/\psi$  forward cross sections. The solid curve employs the MRST HO distributions with  $m = 1.2$  GeV  $\mu/m_T = 2$ , the dashed, MRST HO with  $m = 1.4$  GeV  $\mu/m_T = 1$ , the dot-dashed, CTEQ 5M with  $m = 1.2$  GeV  $\mu/m_T = 2$ , and the dotted, GRV 98 HO with  $m = 1.3$  GeV  $\mu/m_T = 1$ . (Right) Inclusive  $\Upsilon$  production data, combined from all three  $S$  states, and compared to NLO CEM calculations. The solid curve employs the MRST HO distributions with  $m = 4.75$  GeV  $\mu/m_T = 1$ , the dashed,  $m = 4.5$  GeV  $\mu/m_T = 0.5$ , the dot-dashed,  $m = 5$  GeV  $\mu/m_T = 2$ , and the dotted, GRV 98 HO with  $m = 4.75$  GeV  $\mu/m_T = 1$ .

# The Quarkonium $p_T$ Distribution in the $Q\bar{Q}$ NLO Code

Gaussian  $k_T$  smearing,  $\langle k_T^2 \rangle_p = 1 \text{ GeV}^2$  for fixed target  $pp$  and  $\pi p$ , broadened for  $pA$  and  $AA$ , NLO code adds in final state:

$$g_p(k_T) = \frac{1}{\pi \langle k_T^2 \rangle_p} \exp(-k_T^2 / \langle k_T^2 \rangle_p)$$

Comparison with  $J/\psi$  and  $\Upsilon$  Tevatron data at 1.8 TeV shows that the broadening should increase with energy, to  $\langle k_T^2 \rangle_p \approx 2.5 \text{ GeV}^2$

Fits of increase of  $\langle p_T^2 \rangle$  to old data are inadequate to explain this increase so we make a simple linear extrapolation to obtain

$$\langle k_T^2 \rangle_p = 1 + \frac{1}{6} \ln\left(\frac{s}{s_0}\right) \text{ GeV}^2$$

At RHIC energies  $\langle k_T^2 \rangle_p = 1.77 \text{ GeV}^2$  for 200 GeV and  $2.07 \text{ GeV}^2$  for 500 GeV  $pp$  collisions

## Nuclear Effects on $p_T$ Broadening

Additional broadening – beyond the intrinsic broadening – assumed to arise from multiple parton scattering in the target before hard interaction

$J/\psi$ ,  $\Upsilon$  and Drell-Yan show effects of broadening in  $pA$ , parameterized as

$$\langle k_T^2 \rangle_{iA} = \langle k_T^2 \rangle_p + (\langle \nu \rangle - 1) \Delta^2(\mu)$$

The broadening is proportional to the average number of collisions of the projectile parton in the target,

$$\langle \nu \rangle = \sigma_{NN} \frac{\int d^2b T_A^2(b)}{\int d^2b T_A(b)} = \frac{3}{2} \sigma_{NN} \rho_0 R_A$$

$T_A(b)$  is the nuclear profile function

The second equality is average over impact parameter assuming a spherical nucleus,  $\rho_0 = 0.16 \text{ fm}^{-3}$  is the central nuclear density and  $R_A$  is the nuclear radius

$\Delta^2(\mu = 2m)$ , the strength of the broadening, depends on the scale of the interactions

$$\Delta^2(\mu) = 0.225 \frac{\ln^2(\mu/\text{GeV})}{1 + \ln(\mu/\text{GeV})} \text{GeV}^2$$

	$\langle \nu \rangle - 1$	$\Delta^2(\mu)$ ( $\text{GeV}^2$ )
$Q\bar{Q}$	$pA$	central $AA$
$c\bar{c}$	<b>0.35</b>	<b>0.7</b>
$b\bar{b}$	<b>1.57</b>	<b>3.14</b>

## $J/\psi$ $p_T$ Distributions at RHIC

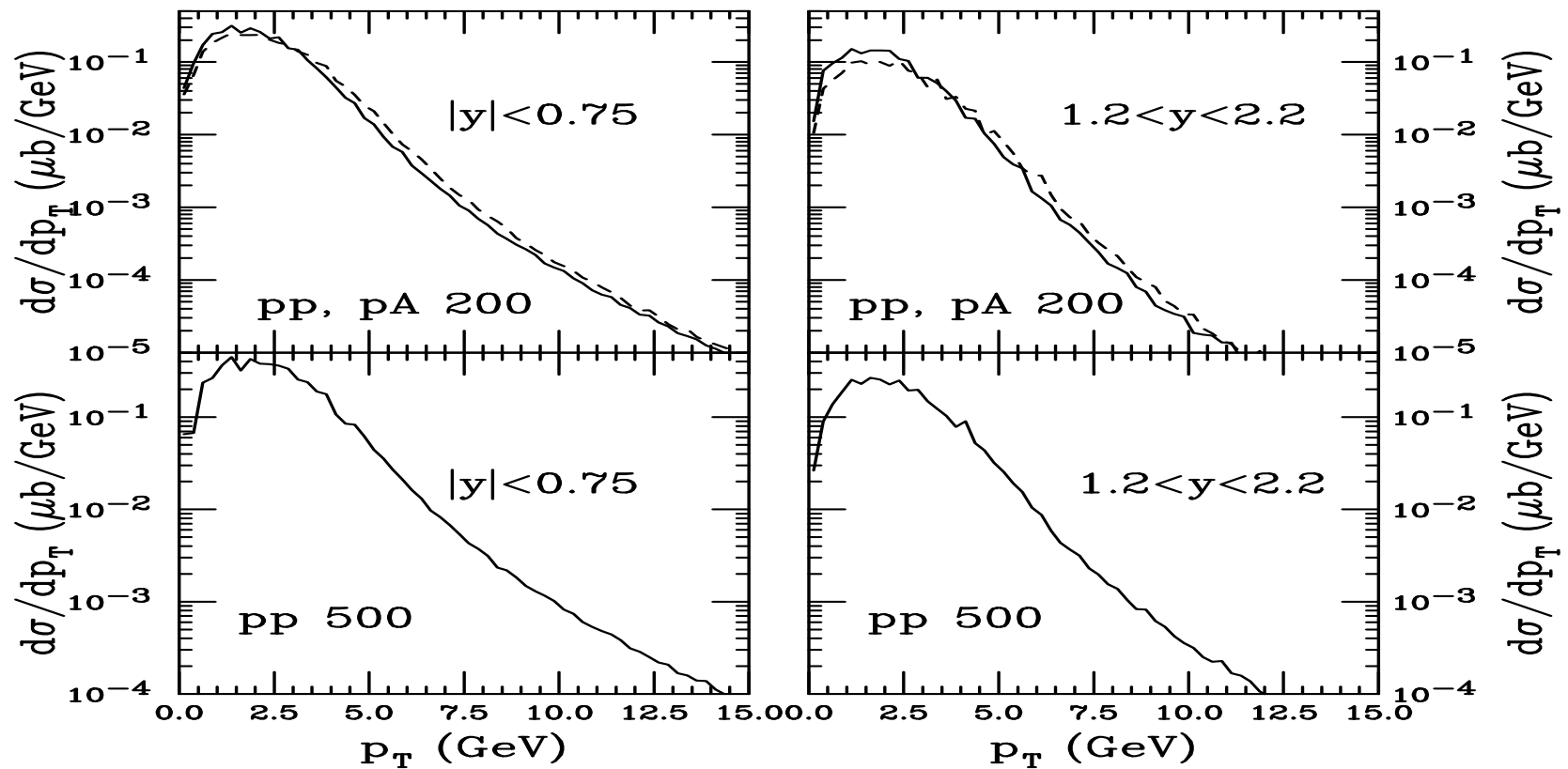


Figure 8: The inclusive  $J/\psi$   $p_T$  distributions at  $\sqrt{s} = 200$  and  $500$  GeV using case  $\psi 1$  (solid). We use  $\langle k_T^2 \rangle_p = 1.77$  GeV<sup>2</sup> for  $pp$  collisions and include broadening in  $pA$  collisions (dashed).

# $\Upsilon$ $p_T$ Distributions at RHIC

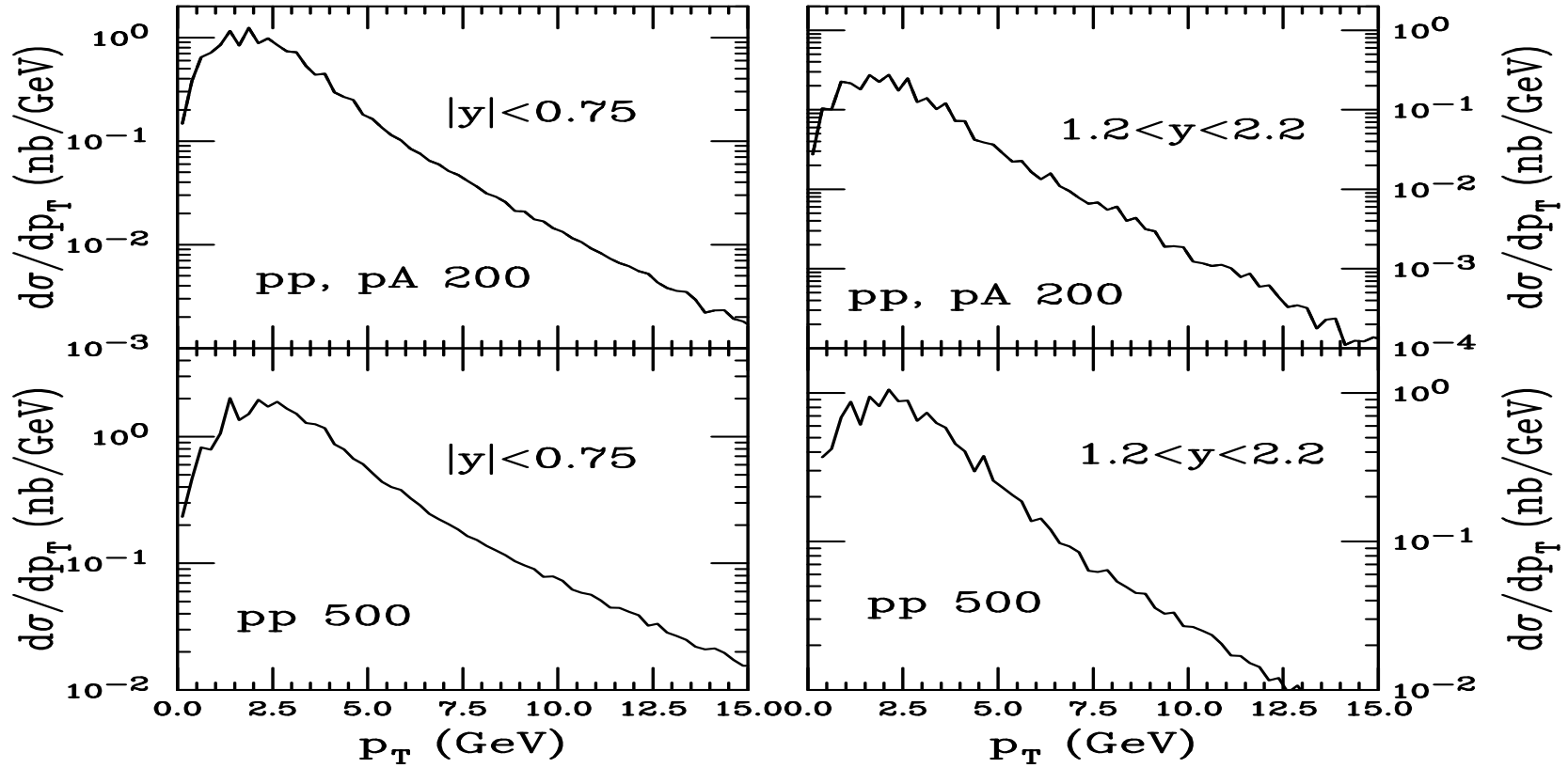


Figure 9: The inclusive  $\Upsilon$   $p_T$  distributions at  $\sqrt{s} = 200$  and 500 GeV for  $m_b = 4.75$  GeV,  $\mu = m_T$  and MRST PDF. We use  $\langle k_T^2 \rangle_p = 1.77$  GeV<sup>2</sup> for  $pp$  collisions.

## $\Upsilon$ Rapidity Distributions at RHIC

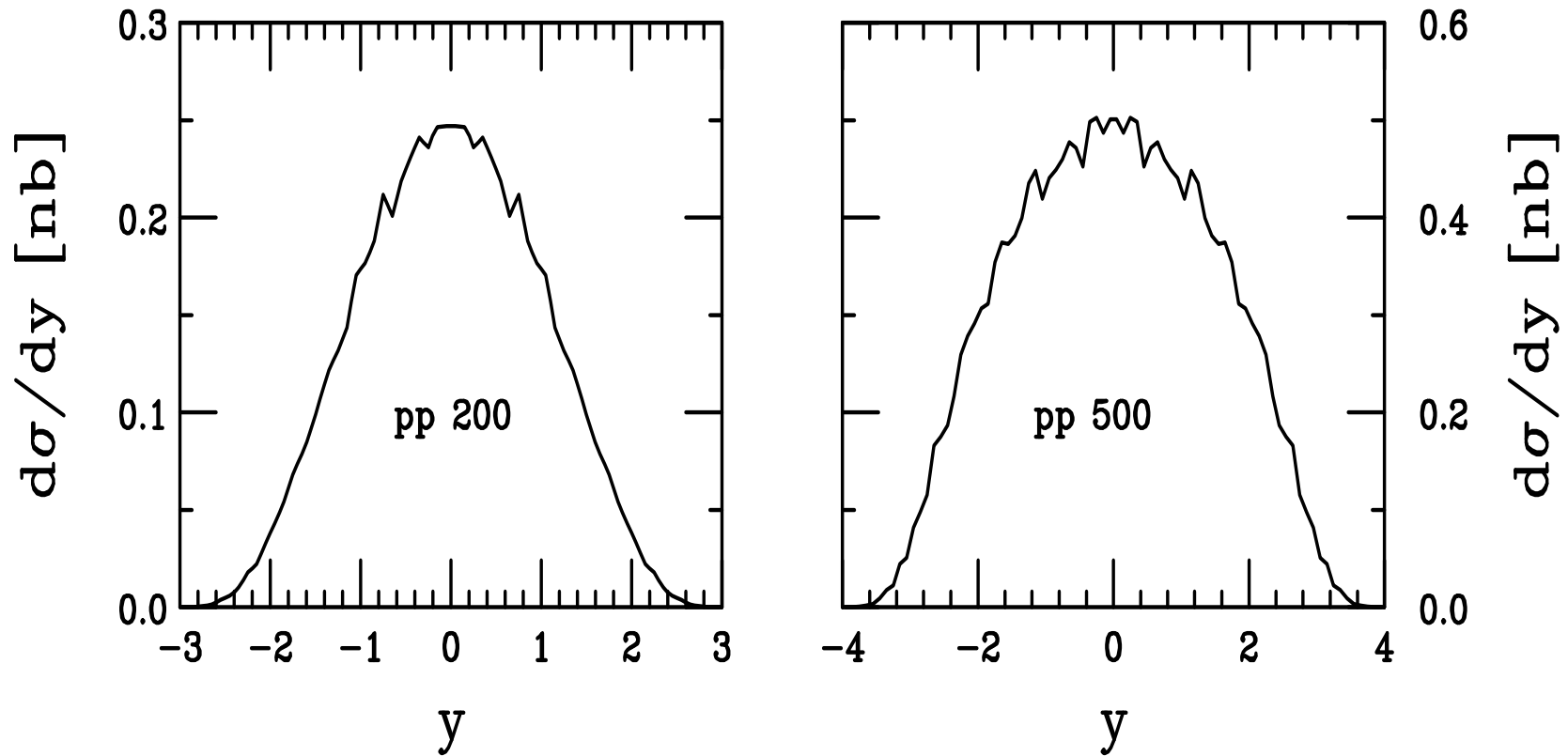


Figure 10: The inclusive  $\Upsilon$   $y$  distributions at  $\sqrt{s} = 200$  and 500 GeV for  $m_b = 4.75$  GeV,  $\mu = m_T$  and MRST PDFs.

# Cold Matter Effects in $p(d,A)+A$ Interactions

Nuclear effects in fixed-target interactions

Parameterizing

$$\sigma_{pA} = \sigma_{pp} A^\alpha \quad \alpha(x_F, p_T)$$

For  $\sqrt{S_{NN}} \leq 40$  GeV and  $x_F > 0.25$ ,  $\alpha$  decreases strongly with  $x_F$  – only low  $x_F$  effects probed by SPS and RHIC rapidity coverage

Consider two low  $x_F$  cold matter effects at colliders:

- Nuclear Shadowing — initial-state effect on the parton distributions affecting total rate, important as a function of  $y/x_F$
- Absorption — final-state effect, after  $c\bar{c}$  that forms the  $J/\psi$  has been produced, pair breaks up in matter due to interactions with nucleons

At high  $x_F$ , other mechanisms (energy loss, intrinsic charm) may be important but  $x_F > 0.25$  corresponds to  $y > 2.8$  at  $\sqrt{S_{NN}} = 200$  GeV (larger  $y$  for higher  $\sqrt{S}$ ) and do not appear in  $p_T$ -integrated  $y$  distributions

# Nuclear Parton Distributions

Nuclear parton densities

$$\begin{aligned} F_i^A(x, Q^2, \vec{r}, z) &= \rho_A(s) S^i(A, x, Q^2, \vec{r}, z) f_i^N(x, Q^2) \\ s &= \sqrt{r^2 + z^2} \\ \rho_A(s) &= \rho_0 \frac{1 + \omega(s/R_A)^2}{1 + \exp[(s - R_A)/d]} \end{aligned}$$

With no nuclear modifications,  $S^i(A, x, Q^2, \vec{r}, z) \equiv 1$

We use Eskola *et al.* (EKS98) and DeFlorian and Sassot (nDSg) parameterizations

Assume spatial dependence proportional to nuclear path length:

$$S_\rho^i(A, x, Q^2, \vec{r}, z) = 1 + N_\rho(S^i(A, x, Q^2) - 1) \frac{\int dz \rho_A(\vec{r}, z)}{\int dz \rho_A(0, z)}$$

**Normalization:**  $(1/A) \int d^2r dz \rho_A(s) S_\rho^i \equiv S^i$ . Larger than average modifications for  $s = 0$ . Nucleons like free protons when  $s \gg R_A$ .

# Comparing Shadowing Parameterizations: $x$ Dependence

EKS98 and nDSg available for all  $A$

EKS98 has strong antishadowing at  $x \sim 0.1$ , nDSg has almost none

EKS98 and nDSg similar for  $A = 208$  but nDSg weaker for smaller  $A$

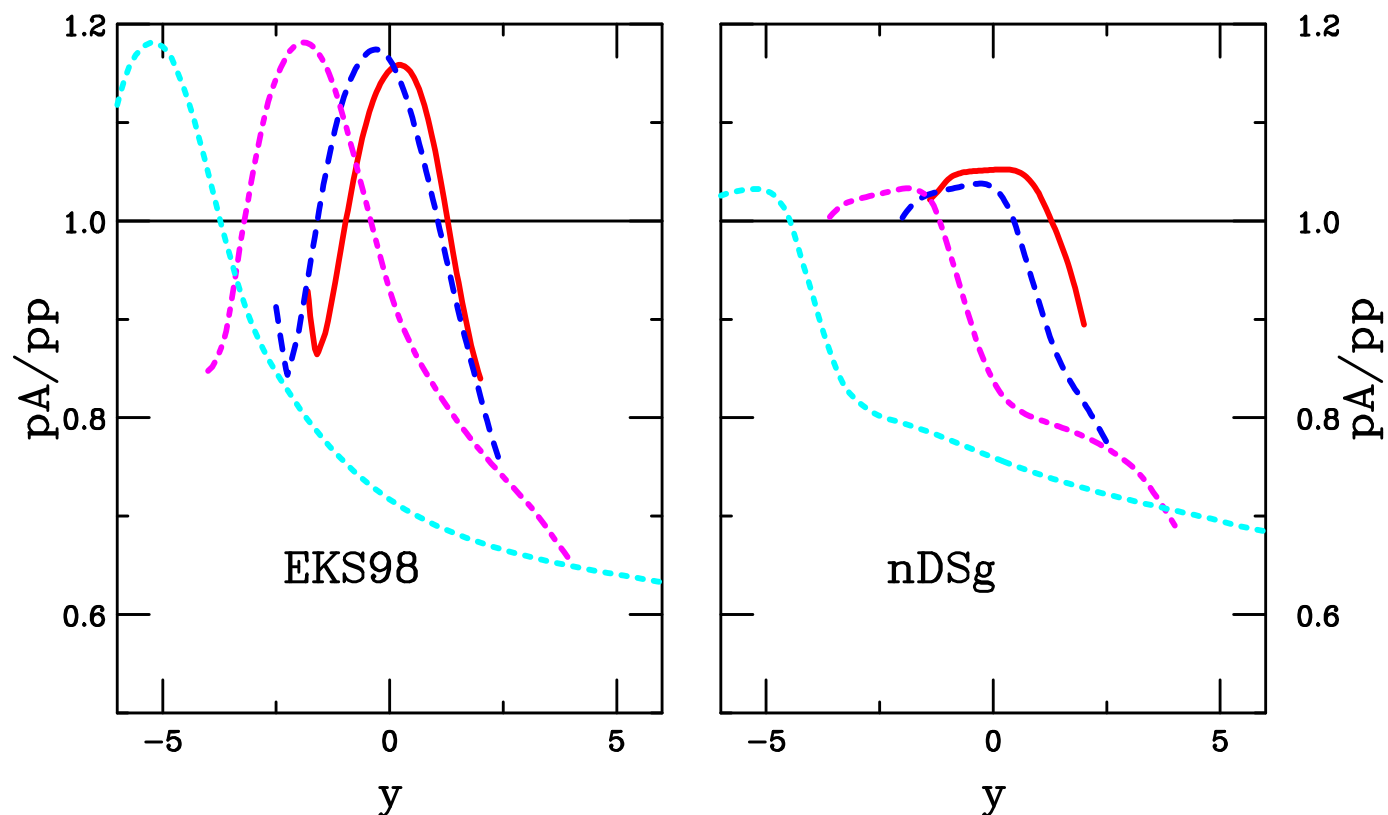


Figure 11: EKS98 (left) and nDSg (right) shadowing ratios as a function of rapidity for  $J/\psi$  production scales with  $A = 200$ . Results are shown for  $\sqrt{S_{NN}} = 20$  (solid), 40 (dashed), 200 (dot-dashed) and 5500 (dotted) GeV.

# Quarkonium Absorption by Nucleons

Woods-Saxon nuclear density profiles typically used

$$\begin{aligned}\sigma_{pA} &= \sigma_{pN} \int d^2b \int_{-\infty}^{\infty} dz \rho_A(b, z) S_A^{\text{abs}}(b) \\ &= \sigma_{pN} \int d^2b \int_{-\infty}^{\infty} dz \rho_A(b, z) \exp \left\{ - \int_z^{\infty} dz' \rho_A(b, z') \sigma_{\text{abs}}(z' - z) \right\}\end{aligned}$$

Note that if  $\rho_A = \rho_0$ ,  $\alpha = 1 - 9\sigma_{\text{abs}}/(16\pi r_0^2)$

The value of  $\sigma_{\text{abs}}$  depends on the parameterization of  $\sigma_{pA}$  – Glauber, hard sphere,  $A^\alpha$  etc. (shown by NA50)

Feed down to  $J/\psi$  from  $\chi_c$  and  $\psi'$  decays included

$$\sigma_{pA} = \sigma_{pN} \int d^2b [0.6S_{\psi, \text{dir}}(b) + 0.3S_{\chi_{cJ}}(b) + 0.1S_{\psi'}(b)]$$

Predictions that quarkonium absorption cross sections decrease with energy (M. A. Braun *et al.*, Nucl. Phys. B 509 (1998) 357 [hep-ph/9707424], A. Capella and E. G. Ferreira, hep-ph/0610313) agree with trend of data

Comparison of SPS and RHIC calculations with absorption *and* shadowing require strong absorption to counter antishadowing at the SPS and weak absorption at RHIC where  $x$  is smaller – absorption likely negligible at the LHC

# A Dependence of $J/\psi$ and $\psi'$ Not Identical

Color octet mechanism suggested that  $J/\psi$  and  $\psi'$   $A$  dependence should be identical — Supported by large uncertainties of early data

Newer, bigger data sets (NA50 at SPS, E866 at FNAL) show difference at midrapidity [NA50  $\rho L$  fit gives  $\Delta\sigma = \sigma_{\text{abs}}^{\psi'} - \sigma_{\text{abs}}^{J/\psi} = 4.2 \pm 1.0$  mb at 400 GeV,  $2.8 \pm 0.5$  mb at 450 GeV for absolute cross sections] — Can only be due to absorption

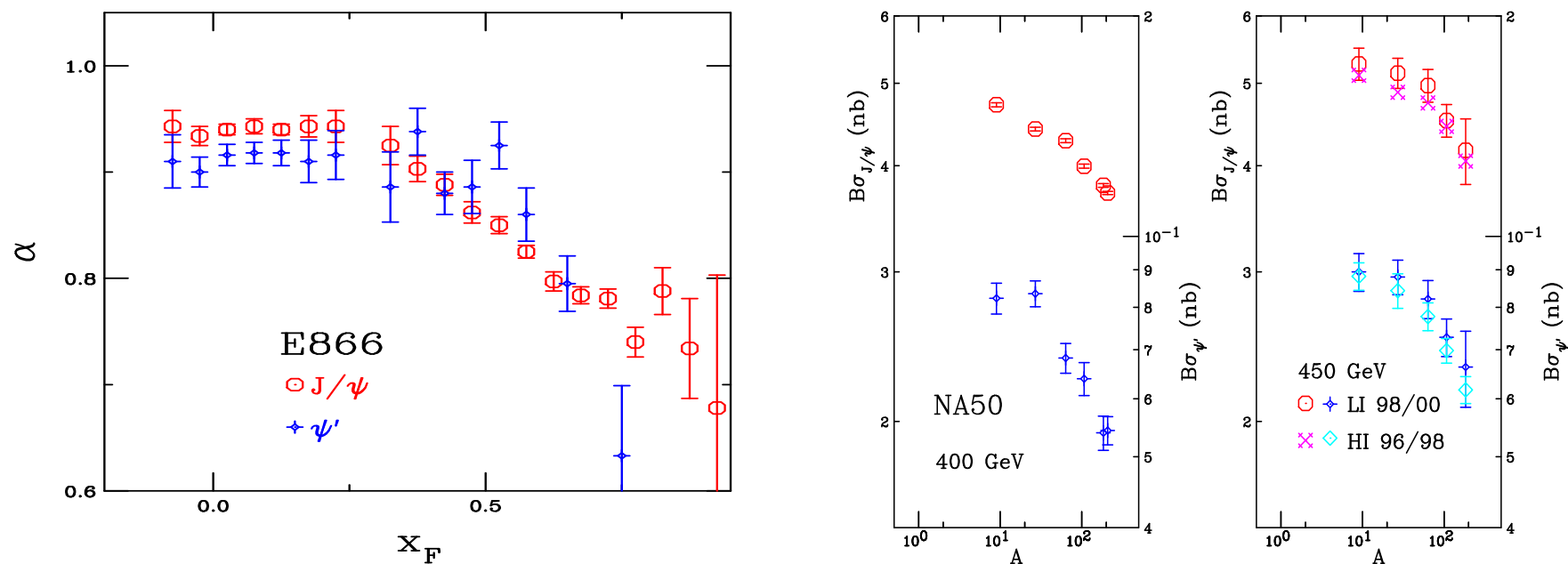


Figure 12: The  $J/\psi$   $A$  dependence (left) as a function of  $x_F$  at FNAL ( $\sqrt{s_{NN}} = 38.8$  GeV) and (right) and a function of  $A$  at the SPS (NA50 at  $p_{\text{lab}} = 400$  and 450 GeV) for  $J/\psi$  and  $\psi'$  production.

# Shadowing and Absorption at the SPS: $A$ Dependence

Stronger antishadowing of EKS98 in SPS midrapidity region calls for bigger absorption cross section

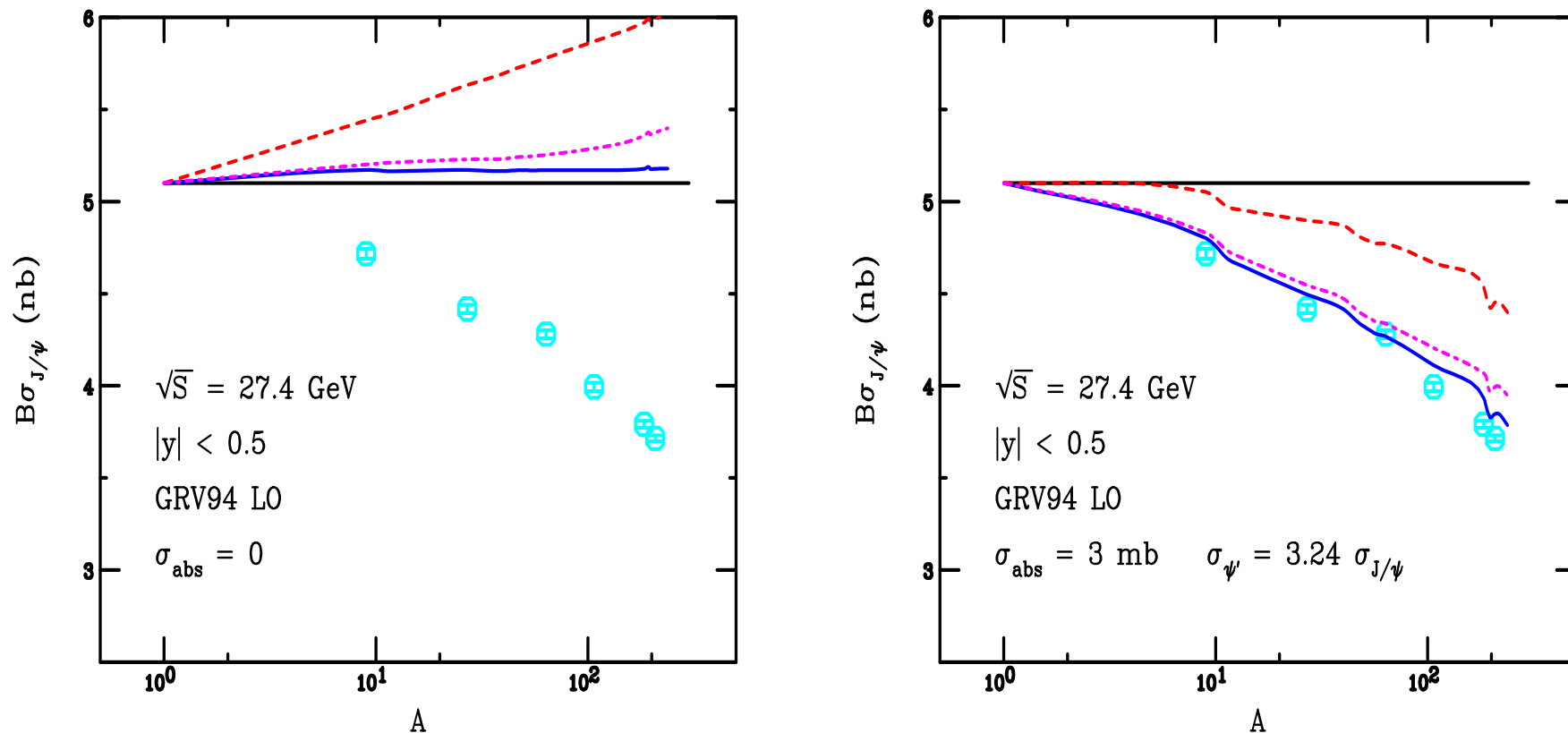


Figure 13: The  $J/\psi$   $A$  dependence at 400 GeV for no absorption (left) and for  $\sigma_{\text{abs}}^{J/\psi} = 3$  mb (right). The curves are with no shadowing (solid blue), EKS98 (magenta dot-dashed) and nDSg (red dashed).

# Predicted $J/\psi$ Rapidity Distributions at RHIC

Agreement of color evaporation model (CEM) with overall normalization of PHENIX data good

Shape has right trend for d+Au with EKS98 shadowing

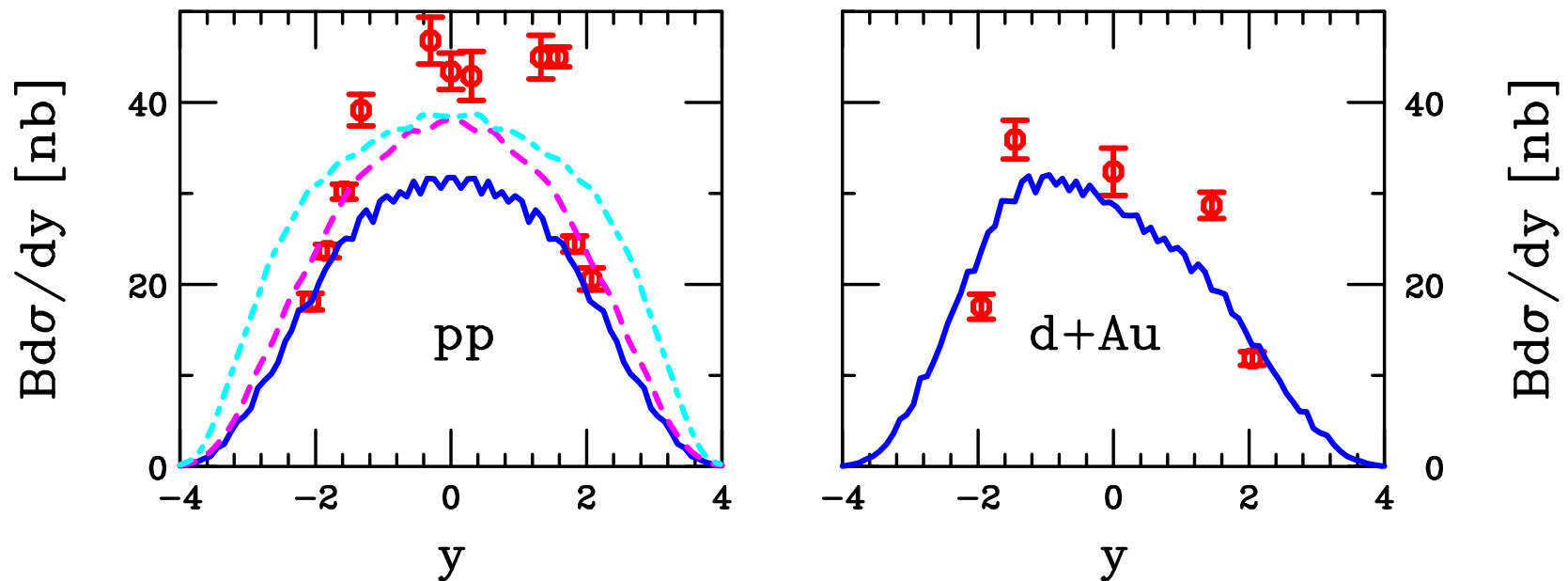


Figure 14: The inclusive  $J/\psi$   $y$  distributions in  $\sqrt{s} = 200$  GeV  $pp$  interactions (left-hand side) calculated with the MRST parton densities in the CEM with  $m_c = 1.2$  GeV,  $\mu = 2m_T$ . The rapidity distribution for d+Au collisions (right-hand side with EKS98) is also shown.

# Absorption and Shadowing at RHIC: $R_{dAu}(y)$

Feed down from higher states with larger absorption cross sections needs  $\sigma_{\text{abs}}^{J/\psi} < 2 \text{ mb}$  with present d+Au data

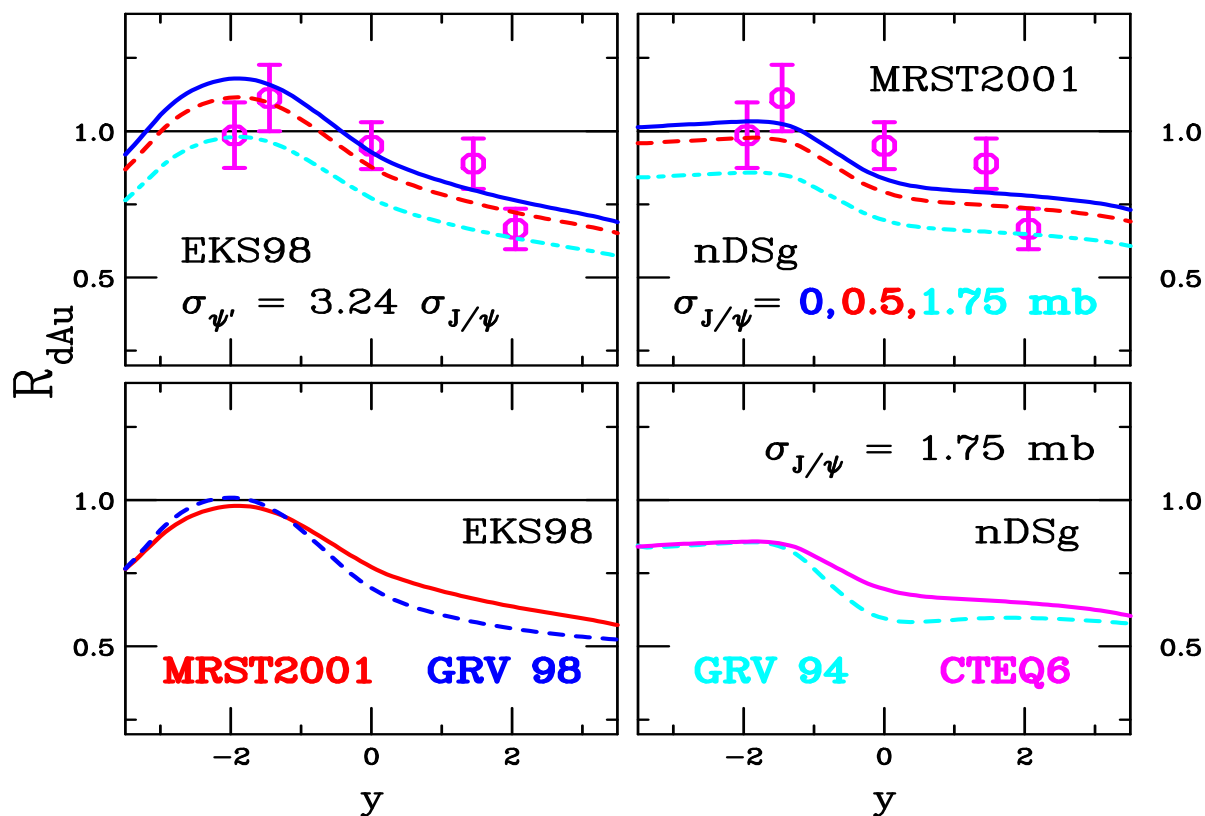


Figure 15: The d+Au/pp minimum bias ratio as a function of rapidity for EKS98 (left) and nDSg (right) parameterizations. The top plots vary the  $J/\psi$  absorption cross section with the MRST2001 PDFs while the bottom plots show the differences in the PDF choice for a fixed absorption cross section.

# Absorption and Shadowing at RHIC: $R_{\text{AuAu}}(y)$

$R_{AA}$  rather flat with rapidity, agreement with data for  $\sigma_{\text{abs}}^{J/\psi} \sim 1 \text{ mb}$

Convolution of shadowing parameterizations give dip at midrapidity

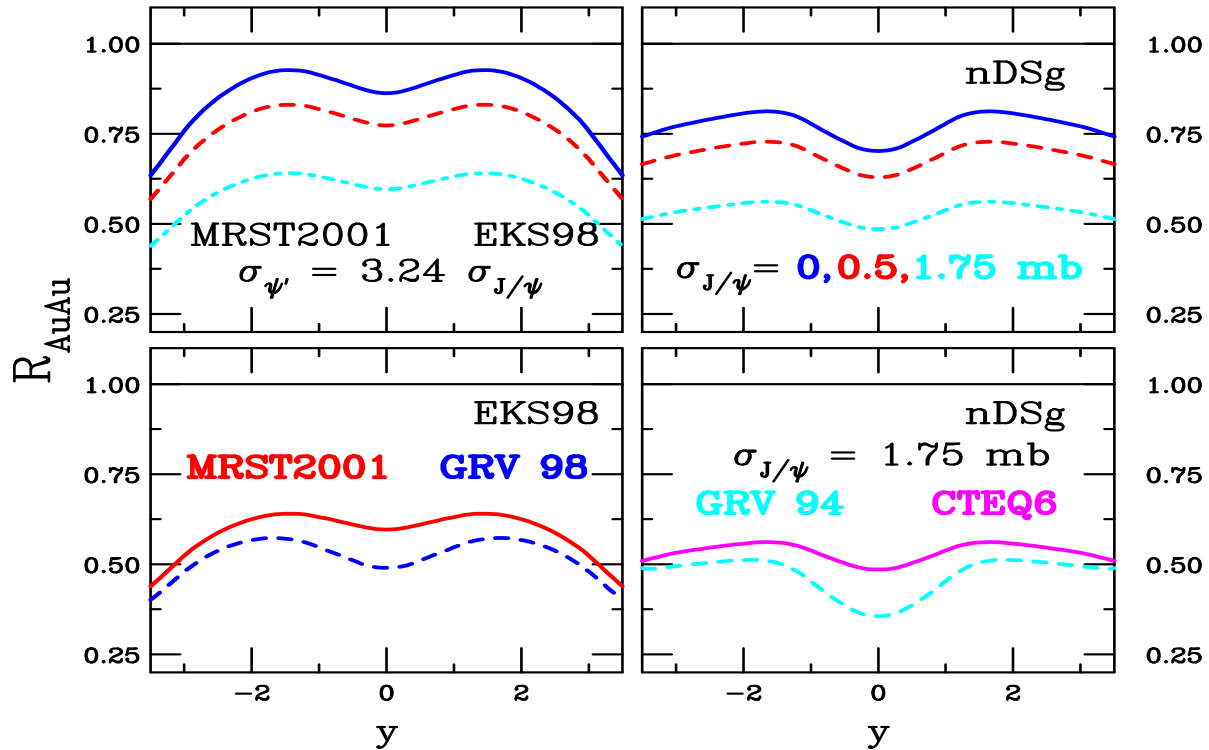


Figure 16: The AuAu/pp minimum bias ratio as a function of rapidity for EKS98 (left) and nDSg (right) parameterizations. The top plots vary the  $J/\psi$  absorption cross section with the MRST2001 PDFs while the bottom plots show the differences in the PDF choice for a fixed absorption cross section.

## Why is $R_{\text{AuAu}}(y)$ higher at $y = 2$ ?

$R_{\text{dAu}}$  is lower at  $y = 2$  than at  $y = 0$  but  $R_{\text{AuAu}}$  is not

Cyan curve is  $R_{\text{Au d}}$ , multiply blue times cyan curves at each  $y$  and get magenta curve, including absorption moves all curves down

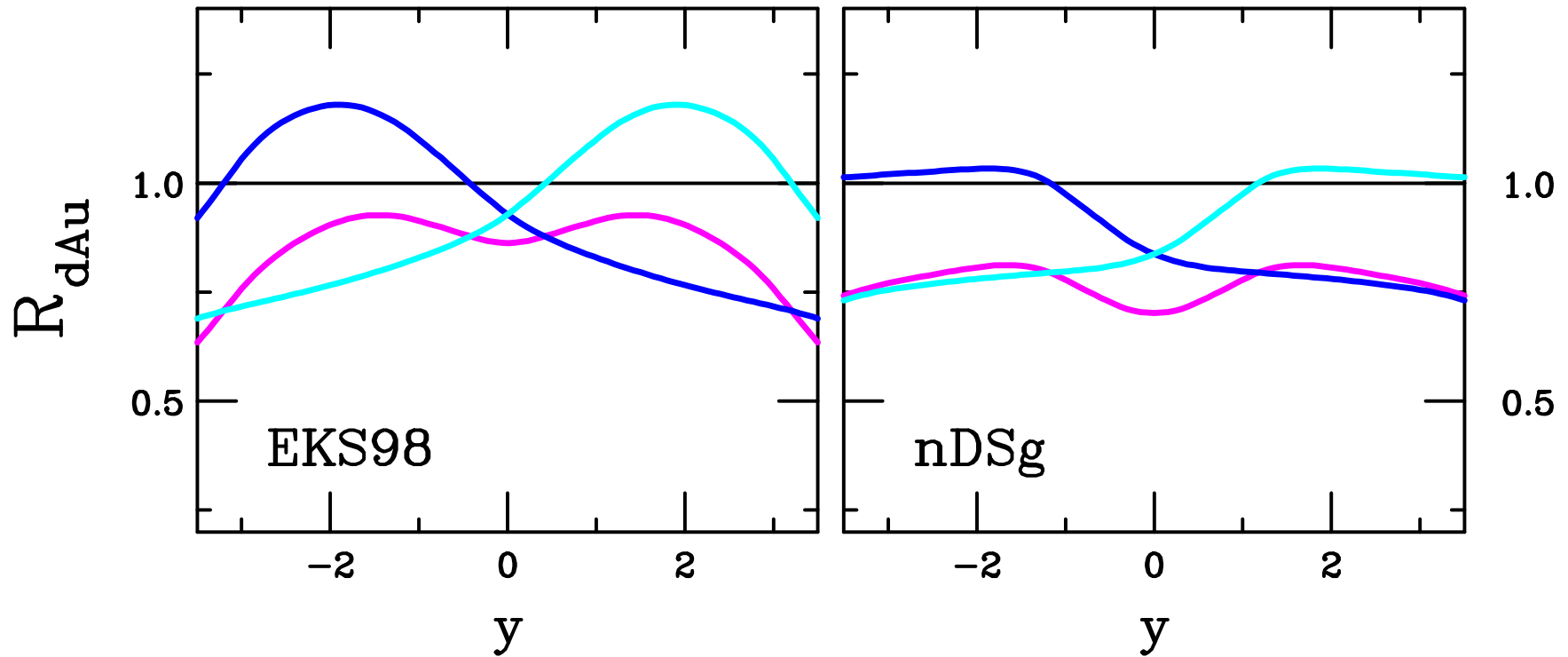


Figure 17: The  $\text{dAu}/pp$  (blue),  $\text{Au d}/pp$  (cyan) and  $\text{AuAu}/pp$  (magenta) ratios as a function of rapidity for EKS98 (left) and nDSg (right) parameterizations with the MRST2001 PDFs.

# How to get $R_{\text{AuAu}}(y = 2)/R_{\text{AuAu}}(y = 0) < 1$

Reduce gluon antishadowing so that  $R_{\text{dAu}} \approx 1$  at  $y = 0$  and shadowing at higher  $y$

This would also require modifying quark shadowing and satisfying momentum sum rule – no parameterization gives this shape – nDSg comes close but shadowing comes before  $y = 0$  and still gives dip at  $y = 0$

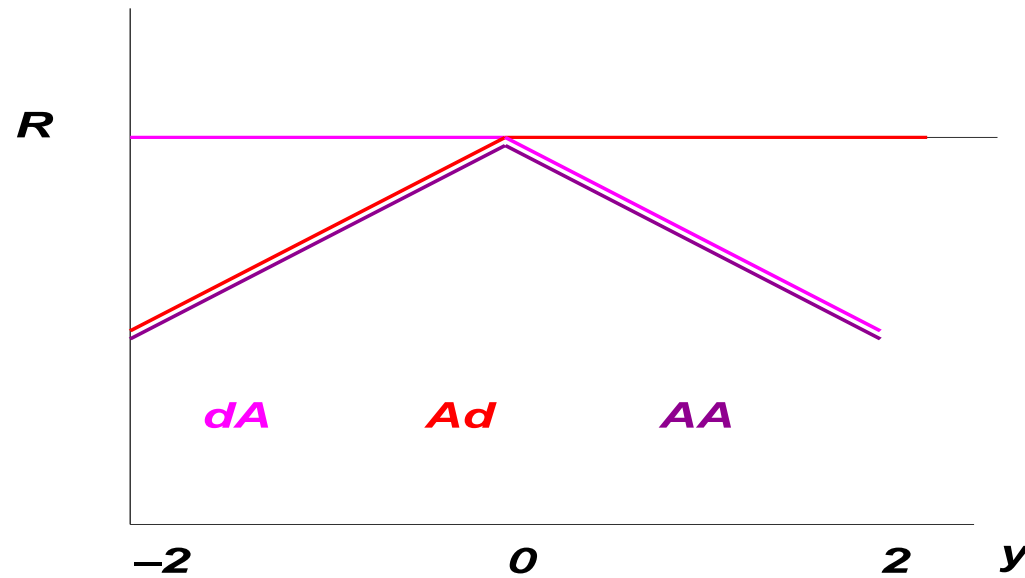


Figure 18: The  $\text{dAu}/pp$  (magenta),  $\text{Au}/pp$  (red) and  $\text{AuAu}/pp$  (purple) ratios as a function of rapidity to make  $R_{\text{AA}}(y = 2)/R_{\text{AA}}(y = 0) < 1$

# Absorption and Shadowing at RHIC: $R_{\text{CuCu}}(y)$

Shadowing reduced for Cu relative to Au

Lower energy Cu+Cu probes larger  $x$ , EKS98 antishadowing peaks coincide at midrapidity

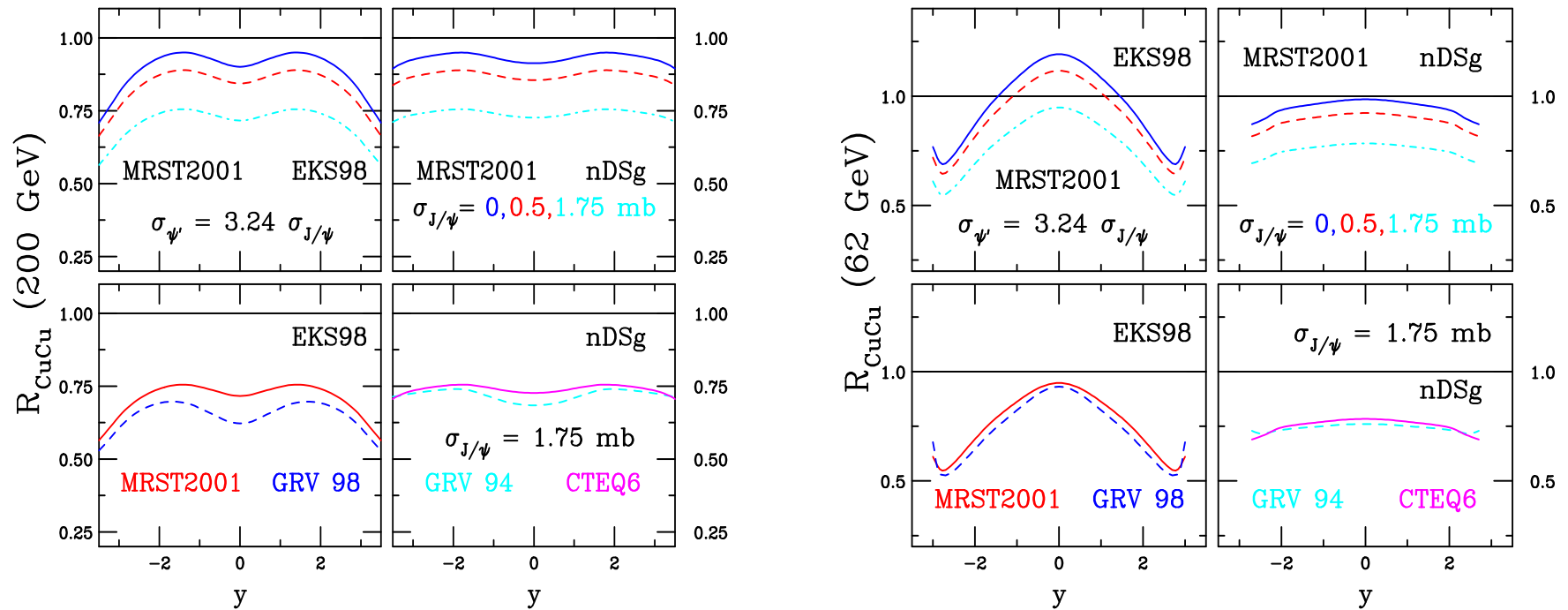


Figure 19: The CuCu/pp minimum bias ratio at 200 GeV (left-hand side) and 62 GeV (right-hand side) as a function of rapidity for EKS98 (left) and nDSg (right) parameterizations. The top plots vary the  $J/\psi$  absorption cross section with the MRST2001 PDFs while the bottom plots show the differences in the PDF choice for a fixed absorption cross section.

## Obtaining $R_{\text{CuCu}}(y)$ at 200 and 62 GeV

nDSg parameterization gives less shadowing for Cu than EKS98

Lower energy shifts  $R_{\text{dCu}}(y)$  toward midrapidity, makes  $R_{\text{CuCu}}(y)$  narrower at 62 GeV

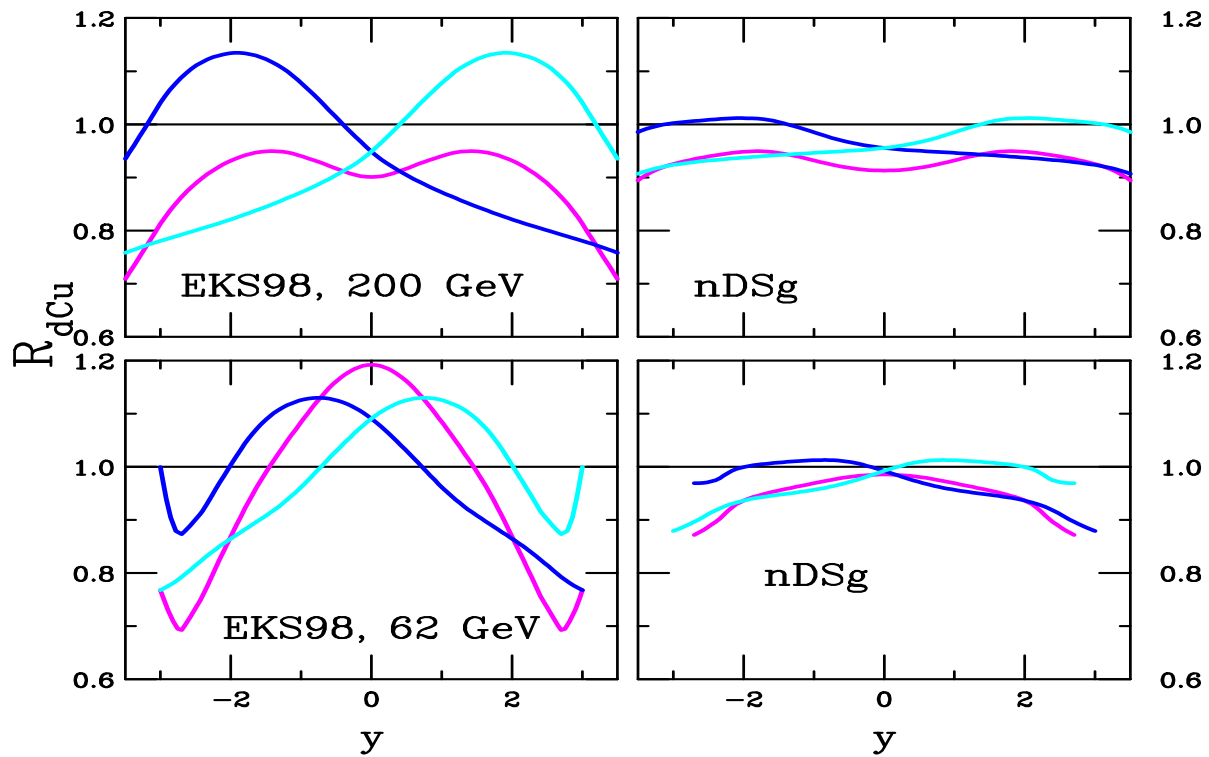


Figure 20: The  $\text{dCu}/pp$  (blue),  $\text{CuCu}/pp$  (cyan) and  $\text{CuCu}/pp$  (magenta) ratios at 200 GeV (left-hand plot) and 62 GeV (right-hand plot) as a function of rapidity for EKS98 (left) and nDSg (right) parameterizations with the MRST2001 PDFs. No absorption effects are included.

# Centrality Dependence of d+Au: $R_{dAu}(N_{coll})$

Largest difference between shadowing parameterizations is in antishadowing region ( $y = -1.7$ ), PDF difference is not large

Data do not strongly distinguish between different  $\sigma_{abs}$

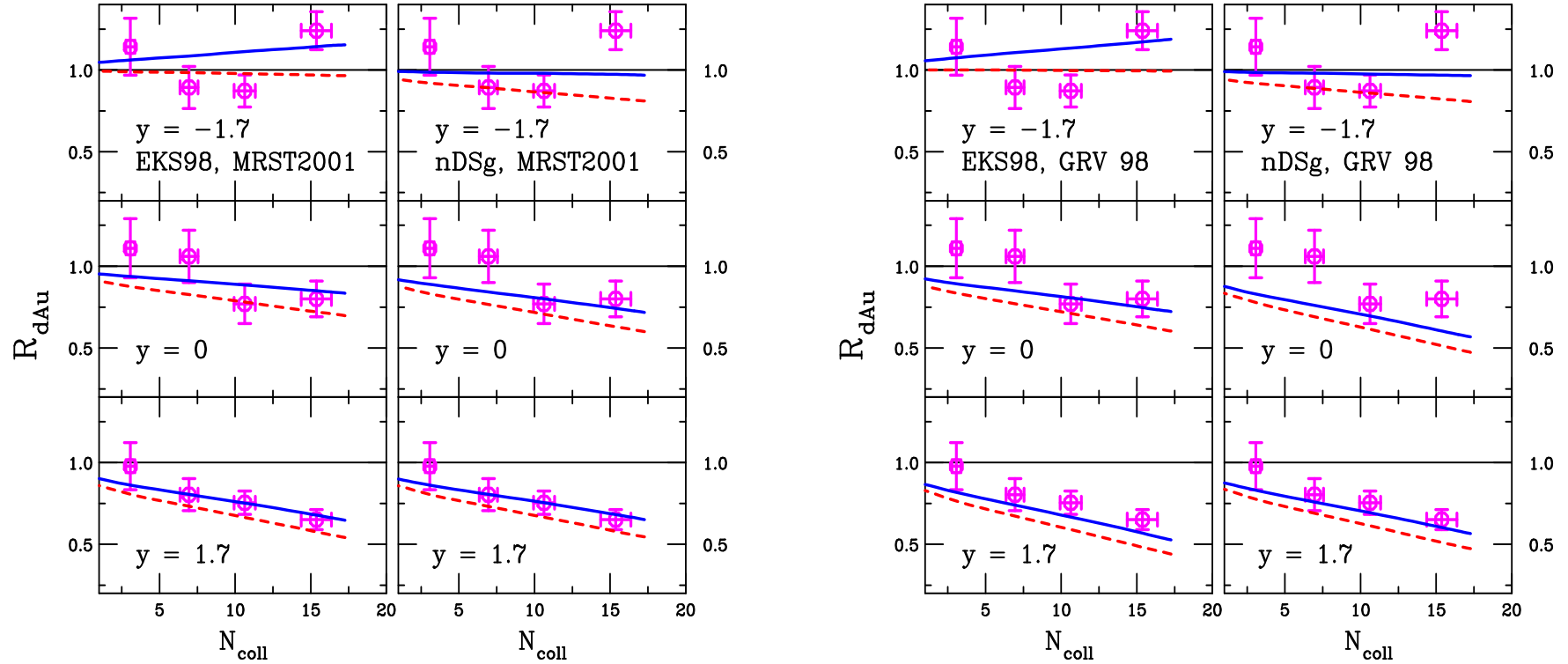


Figure 21: The dAu/pp ratio as a function of the number of collisions calculated with EKS98 (left) and nDSg (right) on each plot with the MRST2001 (left-hand plot) and GRV 98 (right-hand plot) PDFs. The curves are for  $\sigma_{abs}^{J/\psi} = 0.5$  (solid blue) and 1.75 mb (dashed red). PHENIX data are shown for d+Au collisions at 200 GeV for  $y = -1.7$  (top), 0 (middle) and 1.7 (bottom). (An additional 12% overall normalization error is not shown.)

# Centrality Dependence of Au+Au vs $N_{\text{part}}$ : $R_{\text{AuAu}}(N_{\text{part}})$

Cold matter effects with  $\sigma_{\text{abs}} \sim 1$  mb in relatively good agreement with midrapidity data

Stronger  $N_{\text{part}}$  dependence at forward rapidity than predicted

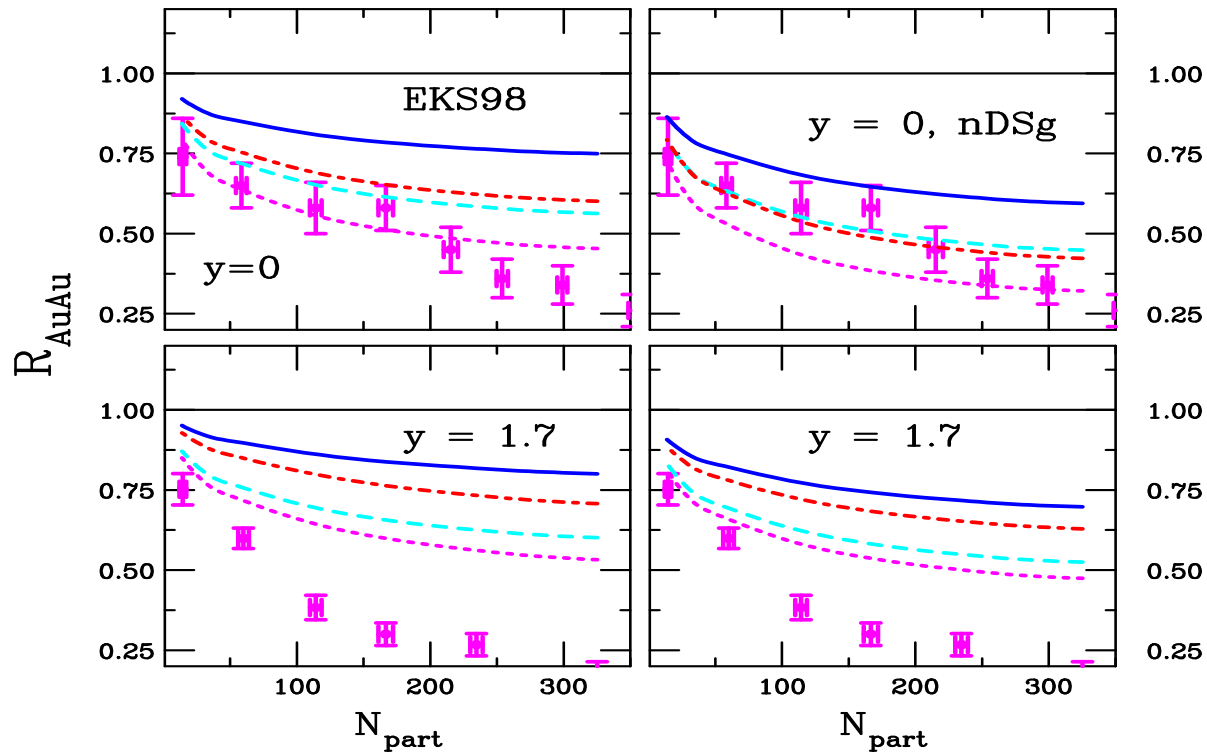


Figure 22: The AuAu/ $pp$  ratio as a function of the number of participants calculated with EKS98 (left) and nDSg (right). The curves are for  $\sigma_{\text{abs}}^{J/\psi} = 0.5$  (solid blue - MRST2001 and dot-dashed red - GRV 98) and 1.75 mb (dashed cyan - MRST2001 and dotted magenta - GRV 98). PHENIX data are shown for Au+Au collisions at 200 GeV for  $y = 0$  (top), and 1.7 (bottom).

# Centrality Dependence of Au+Au vs $y$ : $R_{\text{AuAu}}(y)$ , MRST2001

Shadowing and absorption considerably reduced in peripheral AA

Narrower distributions at midrapidity could be due to regeneration of  $J/\psi$  which vanishes in more peripheral events

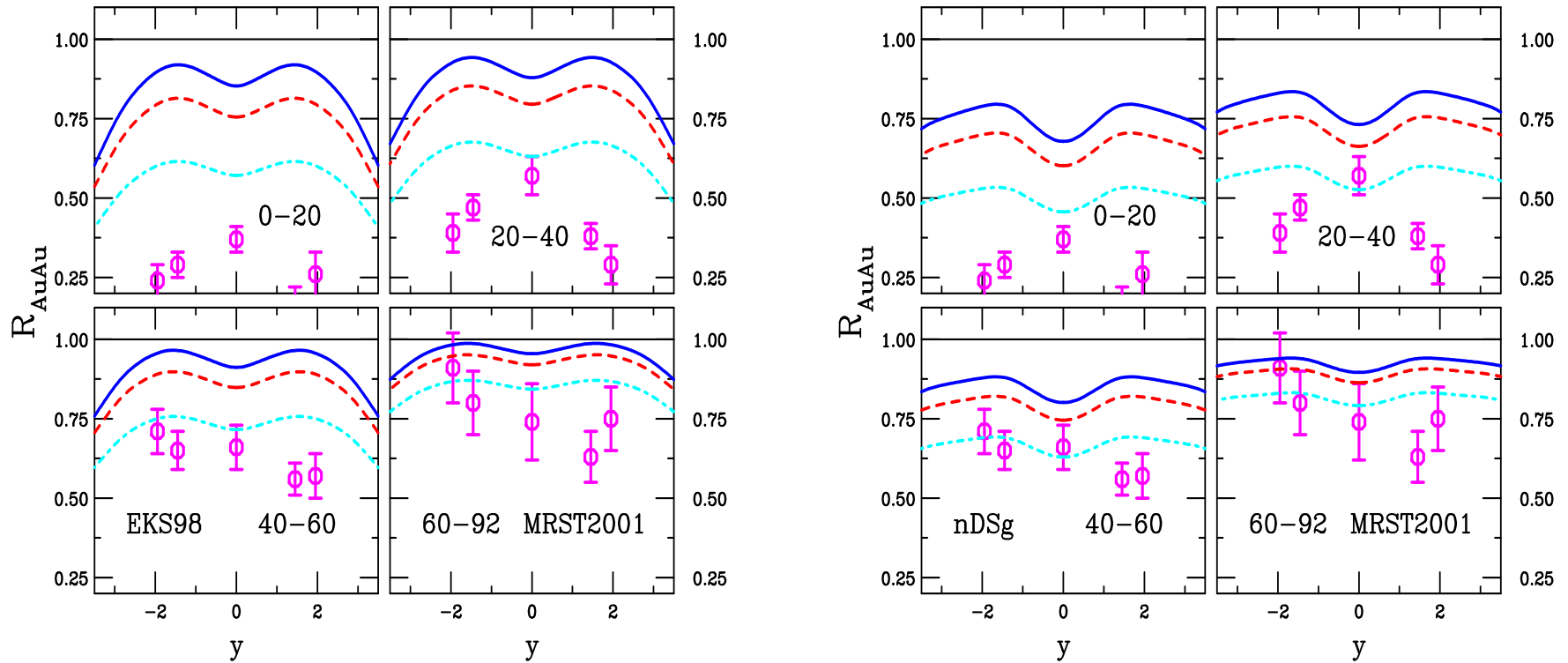


Figure 23: The AuAu/ $pp$  ratio as a function of  $y$  in the four PHENIX centrality bins compared to the data. The calculations with the MRST2001 PDFs are shown with EKS98 (left-hand plot) and nDSg (right-hand plot). The curves are for  $\sigma_{\text{abs}}^{J/\psi} = 0$  (solid blue), 0.5 mb (dashed red) and 1.75 mb (dot-dashed cyan).

# Centrality Dependence of Cu+Cu vs $N_{\text{part}}$ : $R_{\text{CuCu}}(N_{\text{part}})$

Forward results for both energies similar while differences seen at midrapidity

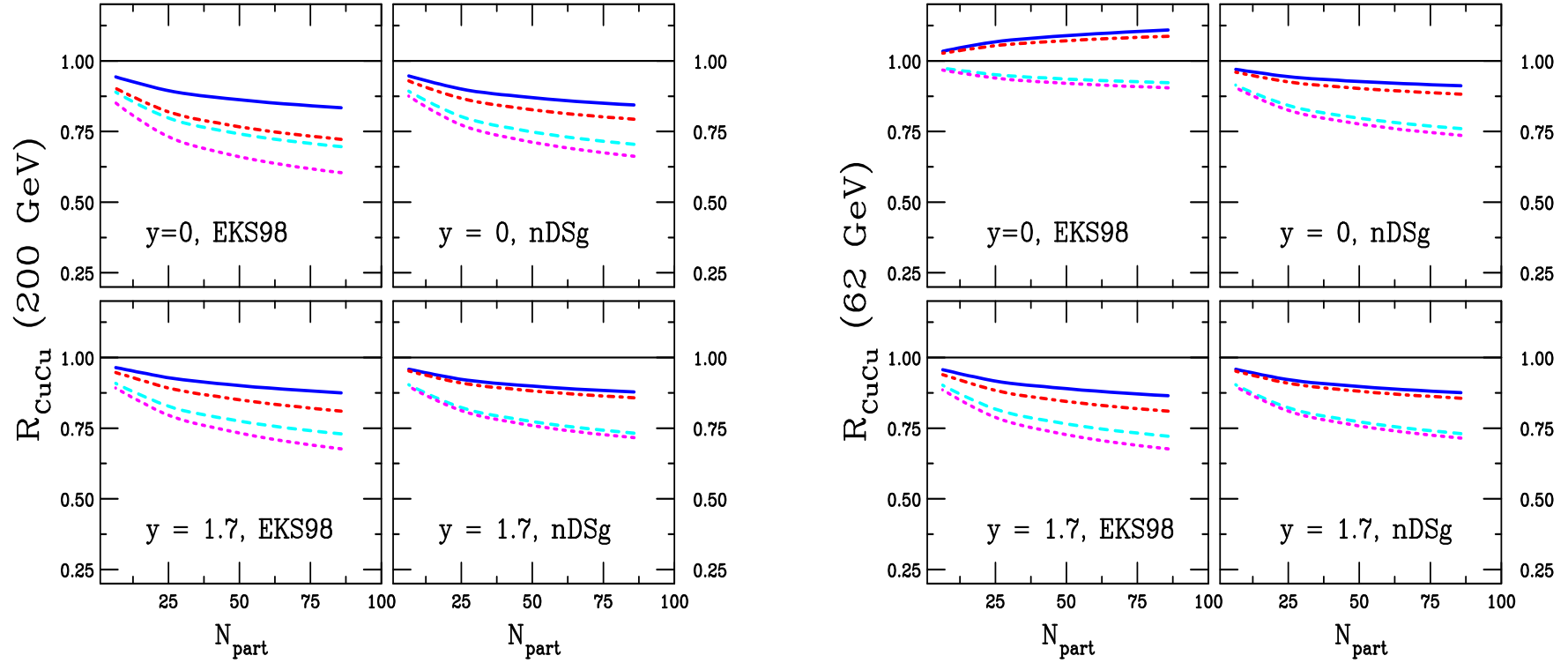


Figure 24: The CuCu/pp ratio as a function of the number of participants for  $\sqrt{s_{NN}} = 200$  (left-hand plot) and 62 (right-hand plot) GeV, calculated with EKS98 (left) and nDSg (right) on each plot. The curves are for  $\sigma_{\text{abs}}^{J/\psi} = 0.5$  (dashed cyan - MRST2001 and dot-dashed red - GRV 98) and 1.75 mb (solid blue - MRST2001 and dotted magenta - GRV 98).

## Summary: Quarkonium .

- SPS data clearly show that  $J/\psi$  and  $\psi'$  have different  $A$  dependence, translates into different effective absorption for  $J/\psi$  and  $\psi'$  – should be checked at RHIC to test apparent decrease of effective absorption
- Measurement of  $\chi_c$   $A$  dependence would provide additional test of absorption mechanism
- Current d+Au  $J/\psi$  data agree well with combination of initial state shadowing and final state absorption
- Need better statistics to distinguish between shadowing parameterizations and determine strength of absorption at RHIC as well as regeneration effect in central and semi-central  $AA$
- Cold matter effects need to be accounted for in  $AA$  collisions but room for dense matter effects .